THE JOURNAL OF BIOLOGICAL CHEMISTRY VOL. 286, NO. 13, pp. 10897–10910, April 1, 2011

Unambiguous Characterization of Site-specific Phosphorylation of Leucine-rich Repeat Fli-I-interacting Protein 2 (LRRFIP2) in Toll-like Receptor 4 (TLR4)-mediated Signaling*[S]

Received for publication, July 26, 2010, and in revised form, December 29, 2010 Published, JBC Papers in Press, January 10, 2011, DOI 10.1074/jbc.M110.168179

Harsha P. Gunawardena[‡], Yi Huang[§], Roma Kenjale[§], Haiyang Wang[§], Ling Xie[§], and Xian Chen[‡§1]

From the [§]Department of Biochemistry and Biophysics and [‡]Program in Molecular Biology and Biotechnology, University of North Carolina, Chapel Hill, North Carolina 27599

In the TLR4 signaling pathways, we previously characterized a signal regulator, LRRFIP2, that modulates the time course-dependent changes in NF-κB activity through its dynamic interaction with the TLR adaptor protein, MyD88. However, little is known about the driving force behind the LPS-inducible dynamics between LRRFIP2 and MyD88. We have therefore designed a multiplex label-free quantitative proteomics method to investigate dynamic changes of LRRFIP2 phosphorylation upon LPS stimulation. Given our observation that LRRFIP2 binds to MyD88 through its serine-rich domain in which most of serine residues have the propensity to be phosphorylated, we used collision-activated dissociation- and electron transfer dissociation-based methods in a complementary manner to unambiguously localize phosphorylation sites in the peptides constituting the serine-rich domain. Among 23 phosphorylation sites identified and first quantified by the label-free approach and then verified by the AACT/SILAC (amino acid-coded tagging/stable isotope labeling in cell culture)-based quantitation method, phosphorylation at serine 202 showed a significant LPS-induced dynamic change during the full-course cellular response to LPS stimulation. The substitution of serine 202 with nonphosphorylated residues by site-directed mutagenesis resulted in a weakened LRRFIP2-MyD88 interaction and a concurrently reduced activity in downstream NF-κB. Taking these results together, phosphorylation at serine 202 was found to regulate the dynamics of the LRRFIP2-MyD88 interaction, which in turn modulated the strength and duration of TLR4 signaling. Strategically, we have demonstrated the importance of precise identification of the biologically relevant phosphorylation site(s) using comprehensive mass spectrometry-based quantitative proteomics approaches in guiding downstream biological characterization experiments, which could otherwise be both time- and cost-consuming for a large number of phosphorylation possibilities.

As the first line of defense, toll-like receptors (TLRs)[2] can sense diverse pathogenic products that activate the innate immune/inflammatory response of the host cells (1–3). TLR4 specifically recognizes lipopolysaccharide (LPS), which is a major component of the Gram-negative bacterial cell wall (1–3). Through mechanisms that have yet to be explored, emerging evidence suggests that LPS-triggered TLR4 signaling is tightly modulated by specific intracellular protein-protein interaction networks or interactomes (1). As an overview of TLR4-mediated signaling (4), upon LPS stimulation, MyD88, the common intracellular adaptor protein located immediately downstream of most TLR molecules (5), can recruit specific intracellular proteins along the MyD88-IRAK-TRAF6-IκB-NFκB signal relay to eventually regulate the activity of downstream transcription factors such as NF-κB (6–8). Using our "dual tagging" quantitative proteomic method for signaling complex analysis (9), we have demonstrated that novel signaling proteins can be systematically identified from LPS-stimulated living macrophages (9, 10).

A class of proteins containing a leucine-rich repeat (LRR) motif has recently been found to play the central role in recognition of diverse pathogen-associated molecules in host innate defense in plants and animals (11). Among our identified MyD88-interacting proteins, there were two LRR-containing proteins (or Fliih-interacting proteins): leucine-rich repeat Fli-I-interacting protein 2 (LRRFIP2) and Fli-I leucine-rich repeat-associated protein 1 (Flap-1). The LRR-containing protein, flightless I homologue (Fliih), was first characterized as a negative mediator of NF-κB activity (9, 10), whereas LRRFIP2 acts as a positive regulator for activating NF-κB during the early host response to LPS stimulation (12). Further, through the combined biological characterization and real-time quantitative measurement of protein interactions, we have shown that, depending upon the length of host exposure to a TLR agonist, multiple proteins, including LRRFIP2, Fliih, and MyD88, interact in a timely and orderly manner during the full course of TLR-mediated signal transduction (12). However, the molecular mechanism remains obscure regarding how LPS-inducible temporal interactions among these signaling proteins are regulated for control of the duration and strength of TLR4 signaling.

* This research was funded, in whole or in part, by National Institutes of Health Grant 1R01A1064806-01A2.

[S] The on-line version of this article (available at http://www.jbc.org) contains supplemental Figs. 1S–4S.

[1] To whom correspondence should be addressed. Tel.: 919-843-5310; E-mail: xianc@email.unc.edu.

[2] The abbreviations used are: TLR, Toll-like receptor; MyD88, myeloid differentiation primary response gene-88; LRR, leucine-rich repeat; CAD, collision-activated dissociation; CID, collision-induced dissociation; ETD, electron transfer dissociation; MS/MS, tandem mass spectrometry; AACT, amino acid-coded tagging; SILAC, stable isotope labeling in cell culture; Ascore, ambiguity score; IT, ion trap; FT, Fourier transform; SRM, single reaction monitoring; XIC, extracted ion chromatogram; bis-Tris, 2-[bis(2-hydroxyethyl)amino]-2-(hydroxymethyl)propane-1,3-diol.

It is estimated that ~20% of the human genome encodes for the proteins involved in signal transduction (13, 14), where dynamic phosphorylation is known to play critical roles through regulating specific protein-protein interactions (15–17). Given that LRRFIP2 contains a serine-rich domain that has a high propensity to be phosphorylated and has also been found to be involved directly in LRRFIP2-MyD88 interaction (12), we reasoned that specific phosphorylation(s) may show dynamic changes in the MyD88-interacting domain of LRRFIP2 in an LPS-inducible manner to regulate the temporal interactions between these two proteins.

Emerging mass spectrometry (MS)-based techniques can quantify phosphorylation changes in response to cellular perturbations that impinge upon particular biological systems (18). We previously introduced a quantitative proteomics strategy of amino acid-coded tagging (AACT) (19, 20), or SILAC as named by another group (21), and have used it to identify the ionizing radiation-induced phosphorylation of serine 139 of a histone protein, H2AX (22). However, the quantitative capacity of AACT-based approaches is restricted by its cell culture step and maximum 3-plex design in a single experimental run (23).

Without the need for additional chemical reactions or cell culture, emerging MS-based technology for label-free quantitation has no bearing on the number of experimental samples (*i.e.* a label-free approach in principal can capture an infinite number of data points for a multiplex comparative analysis). Currently available software tools for label-free quantitation methodologies measure either spectral counts or the peak area of a given peptide (24). The relative quantitation is achieved by making comparisons of either peak area or spectral counts across multiple mass spectra. At present, label-free quantitation experiments require a high degree of chromatographic reproducibility because data alignment is usually a prerequisite. In addition, sample preparation protocols, data normalization, and statistical validation are required for accurate and precise quantitation. However, label-free technology for quantifying phosphorylation changes can be a cost- and time-effective methodology when large sample sets are involved in any time course study.

In addition to the need for multiplex and precise quantitation, unambiguous identification of site-specific phosphorylation becomes very critical for guiding and minimizing the time- and cost-consuming concurrent experiments for functional characterization of large numbers of phosphorylation sites. Most often, protein modifications have been determined either by identification or by localizing the site of modification by MS/MS of proteolytic peptides (25–29). Ion trap-based mass spectrometers such as the hybrid LTQ Orbitrap have enabled the structural interrogation of the phosphoproteome (30). The facile loss of a structurally uninformative phosphoric acid in ion trap collision-activated/-induced dissociation (CAD/CID)-MS/MS is a major impediment for peptide sequence analysis. Data-dependent, phosphospecific CAD-MS^3 is an efficient strategy for obtaining the spectra of labile phosphopeptides (31). The concurrent activation of a phosphopeptide and its neutral loss product ions via a phosphorylation-dependent pseudo-MS^3 has assisted in the localization of phosphorylation sites (32). However, a recent study has shown that incorrect phosphorylation site assignment is possible for peptides containing multiple serine or threonine residues because of a gas phase rearrangement of the phosphate group during in-trap CAD (33). In this regard, electron-based dissociation methods such as electron capture dissociation (ECD) and electron transfer dissociation (ETD) have been developed for the accurate localization of phosphorylation sites due to the preservation of labile bonds while efficiently cleaving the N–C_α bonds of a peptide (34–37). The ETD technology has been implemented for peptides separated on a chromatographic time scale in standalone ion traps, high resolution and accurate mass hybrid instruments such as the ion trap-Orbitrap (38). The emergence of bioinformatics tools to analyze data from these technology developments has further improved the precision of large scale phosphoproteomics analysis (39, 40).

Here we demonstrate a comprehensive workflow that includes multiplex targeted label-free quantitation and complementary ion dissociation methods for both accurate quantitation and precise identification of those residues of LRRFIP2 showing the LPS-inducible and time course-dependent phosphorylation changes. Using various biological approaches, we have elucidated the possible functional role of novel phosphorylation site(s) precisely identified by quantitative MS-based approaches. Our discovery-based strategy is fully illustrated by the precision with which the phosphorylation sites have been localized; the biological significance of the quantitative threshold and the dynamic phosphorylation changes are closely correlated with the functional role of LRRFIP2 in TLR4 signaling (*i.e.* the site-specific phosphorylation changes or the lack thereof correlates with the LPS-induced changes or lack thereof in the key components of the TLR4-mediated signal transduction involved in LRRFIP2-MyD88 interaction and downstream NF-κB activation). The results of our biological experiments further illustrate the accuracy of our discovery-based mass spectrometry workflow.

EXPERIMENTAL PROCEDURES

Reagents and Materials, Cell Culture/Transfection, Immunoprecipitation, and AACT Labeling—LPS (from *Escherichia coli* 0111:B4, Ultra-pure) were purchased from InvivoGen. Anti-FLAG (M2) and anti-HA were from Sigma-Aldrich. The HEK293T cell line stably expressing TLR4 (both labeled and unlabeled) was cultured as described previously (9, 10). HEK293T/TLR4/MD-2 cells were transfected with plasmid expressing FLAG-tagged LRFFIP2 using Lipofectamine 2000 (Invitrogen) as described previously (12). At 24 h post-transfection, the cells were stimulated with 1 ng/μl LPS-B4 and collected at different time points. With a higher transfection efficiency, the RAW cell transfections were done by using jetPRIME transfection reagent from Polyplus (New York, NY) according to manufacturer's directions. The whole-cell lysates for each time point, containing ~6–10 million cells, were pretreated with mouse IgG and protein G-agarose. FLAG-tagged LRRFIP2 was immunoprecipitated from supernatants with mouse monoclonal anti-FLAG M2 antibody-agarose (Sigma-Aldrich). Immunoprecipitates were eluted with 1× SDS gel loading buffer and separated on NuPAGE 4–12% bis-Tris gel (Invitrogen). In-gel digestion was performed on the protein

bands of interest (41). For multiplex label-free experiments, using anti-FLAG antibody, the same immunoprecipitation procedure as described above was performed to isolate the "snapshot" FLAG-tagged LRRFIP2 from the TLR4 stable HEK cells collected at different time points including 0, 1, 5, 10, 20, and 60 min following LPS stimulation.

AACT/SILAC labeling of the 293T-TLR4 cells was carried out based on the protocol described previously (9, 10). In this case, the nonstimulated cells were labeled with Leu-d_3, whereas the unlabeled cells were stimulated for 10 min with LPS. FLAG-tagged LRRFIP2 was immunoprecipitated from the cell lysate of each labeled or unlabeled cells before mixing at a 1:1 ratio.

Mass Spectrometry Analysis—Samples were desalted using PepClean C18 spin columns (Pierce) according to manufacturer's directions and resuspended in an aqueous solution of 0.1% formic acid. Analysis of most samples was performed via reversed phase LC-MS/MS using a two-dimensional nanoLC-Ultra system (Eksigent Technologies, Dublin, CA) coupled to an LTQ Orbitrap XL system with ETD (Thermo Scientific). The Eksigent system was configured to trap and elute peptides in the one-dimensional mode of operation via a sandwiched injection of ~250 fmol of sample. The trapping was performed on a 3-cm long, 100-μm inner diameter C18 column, and elution was performed on a 15-cm long, 75-μm inner diameter, 5-μm, 300 Å particle (ProteoPep II integraFrit C18 column, New Objective Inc., Woburn, MA). Analytical separation of all the tryptic peptides was achieved with a linear gradient of 2–40% buffer B over either 70 or 120 min at a 200 nl/min flow rate, where buffer A is an aqueous solution of 0.1% formic acid and buffer B is a solution of acetonitrile in 0.1% formic acid.

Mass spectrometric data acquisition was performed in a data-dependent manner on a hybrid LTQ Orbitrap mass spectrometer. A full-scan mass analysis on an Orbitrap (externally calibrated to a mass accuracy of <1 ppm and a user-defined resolution of 30,000) was followed by intensity-dependent MS/MS of the top six most abundant peptide ions in the linear ion trap. CAD-MS/MS and ETD-MS/MS were used as complementary methods to dissociate peptides. All CAD-MS/MS spectra were obtained for peptide ions that were subjected to 30 ms resonance activation at normalized collision energy of 35 eV in the presence of helium bath gas atoms at a pressure of 1 mtorr. All ETD-MS/MS spectra were obtained by performing an ion/ion reaction between peptide cations and fluoranthene anions mutually stored for 100 ms within a linear ion trap. The MS/MS acquisition of a precursor m/z was repeated for a 30-s duration and subsequently excluded for 60 s. Monoisotopic precursor ion selection and charge state screening were enabled to trigger data-dependent MS/MS scans. A few neutral H_3PO_4 loss-dependent CAD-MS^3 experiments and targeted peptide CAD-MS/MS experiments were also performed.

The AACT samples were identified by a MALDI-TOF/TOF 4700 proteomics analyzer (Applied Biosystems, Framingham, MA). Mass spectra were obtained using a 200-Hz Nd:YAG laser operating at 355 nm. External calibration was performed before each run using a myoglobin digest. CAD-MS/MS was performed with a collision voltage of 1 kV with air as the collision gas. Spectra were accumulated for 2000–3000 consecutive laser shots. A mixture of 2,5-dihydroxybenzoic acid (30 $mg \cdot ml^{-1}$, 0.5 μl) and phosphoric acid (1%, 0.5 μl) was used as the MALDI matrix. Mass spectra were processed, and peptide identification was performed using Mascot (Matrix Science Inc.) and Sequest (Thermo Fisher Scientific) search algorithms against a human-IPI (international protein index) database (version 3.63). Peptides were confidently identified using a target-decoy approach with a false discovery rate of 1%. A precursor ion mass tolerance of 100 ppm and a product ion mass tolerance 0.5 Da were used during the search with a maximum of two missed trypsin cleavages. Variable modifications included methionine oxidation and phosphorylation at serine, threonine, and tyrosine residues. A few searches were also carried out using C-terminal sodiation and deamidation at asparagine residues. The Ascore algorithm was used to confidently localize the phosphorylation site on the peptide.

Peptide Quantitation—Label-free quantitation was based on relative peak areas of the identified phosphopeptides and corresponding nonphosphopeptide counterpart. The raw peaks were processed, and extracted ion chromatograms (XIC) were generated from the full-scan MS using Xcalibur software. Peptide peaks of interests were normalized by internal standard peak areas of a tryptic peptide derived from a digest of bee venom mellitin (Sigma-Aldrich), and introduced into each sample during LC-MS analysis. The variations in electrospray ionization (ESI) response were normalized by the response of the dioctyl phthalate ions (m/z 391.28) used as a reference standard. The integration of each analyte data point was performed using the Genesis algorithm (Thermo Fisher Scientific). The normalization of each analyte data point with a corresponding data point of the reference standard was performed using a PerlScript that was written in-house. All deviations in retention time were corrected by peak alignment. The accuracy of the peak area ratios was validated by acquiring multiple chromatographic runs at 90 and 120 min with the linear gradients described above. Label-free quantitation of phosphorylation is based on site occupancy and requires a summation of the peak areas of all phosphopeptides and nonphosphopeptide counterparts comprising the putative phosphorylation site. The percentage of the normalized phosphorylation level for a given site is shown in Equation 1, where M is the peptide sequence of interest and n is the charge state. It is noteworthy that % phosphorylation does not reflect the "true" percentage of phosphorylation but rather a normalized level.

$$\%\ \text{Normalized phosphorylation} = \frac{\sum_{n=1}^{n=3} \text{area}_{\text{norm}}[M + nH + PO_3]^{n+}}{\sum_{n=1}^{n=3} \text{area}_{\text{norm}}[M + nH + PO_3]^{n+} + \text{area}_{\text{norm}}[M + nH]^{n+}} \quad \text{(Eq. 1)}$$

The following degenerate forms of peptide M include the semi-tryptic peptides, methionine oxidation, and asparagine deamidation. The peak area is summed across all degenerate forms, charge states, and adduct ions of a peptide. The quantitation methodology was applied to LC-MS data collected for each LPS

stimulation time point. Multiple technical and biological replicates were analyzed for statistical validation of results.

AACT-based quantitation was performed on Leu-d_3/Leu-d_0 doublet peaks and Arg-0/Lys-0, Arg-6/Lys-4, and Arg-10/Lys-6 dual tagged triplet peaks, respectively. Each peak was processed using standard peak filtering criteria, searched using Mascot according to the method described above, and quantified using Mascot distiller inscribed with the appropriate quantitation method.

Site-directed Mutagenesis—Site-directed mutagenesis of full-length FLAG-LRRFIP2 in pCS2 vector was performed using the QuikChange site-directed mutagenesis kit (Stratagene, La Jolla, CA). To change the selected serines to alanines, we used the following synthetic oligonucleotides: CTG AGA AGT GCC *GCT* CTG GCA TCA TTG (Ser-202 → Ala), CTG GTC TGC TGA GAA GTG CCG AGC TGG CAT CAT TGT ACA ATG G (Ser-202 → Glu), and ATT TGC AGT AGG *AGC* GGC CCT GTC ACT (Ser-190 → Ala). We used the oligonucleotides for Ser-190 → Ala and the plasmid LRRFIP2 S202A as the template to make the double mutant S190A,S202A (Ser-190 → Ala and Ser-202 → Ala).

LRRFIP2 Knockdown, RT-PCR, and Expression of LRRFIP2 Constructs in RAW264.7 Cells—RAW264.7 cells were transfected with an shRNA construct (12) targeting the endogenous mouse *LRRFIP2* gene or scrambled shRNA as a negative control using jetPRIME transfection reagent. The human wild-type and mutant LRRFIP2 constructs were prepared using the QuikChange (Agilent, Santa Clara, CA) site-directed mutagenesis kit in the shRNA binding region, resulting in nucleotide changes but preserving the amino acid sequence. Thus, with the shRNA construct, we could achieve knockdown of endogenous mouse *LRRFIP2* but not the transfected human LRRFIP2 constructs.

Total RNA was prepared from RAW264.7 cells cultured in 24-well plates using the GeneJet RNA purification kit (Fermentas Inc., Glen Burnie, MD), and first-strand synthesis was done with MMLV reverser transcriptase (Promega, Madison, WI). Quantitative real-time polymerase chain reaction was performed by using real-time SYBR Green reagent (Fermentas Inc.) with gene-specific primers on the 7300 Real-time PCR System (Stratagene). Measurements were done in triplicate.

Equal numbers of RAW264.7 cells were transfected with empty vector, wild-type LRRFIP2, or the LRRFIP2 mutant constructs. As the transfection efficiency of RAW cells is much lower than the HEK293T cells, we detected only very weak LRRFIP2 expression in whole-cell lysates, which were not reproduced as an image. Thus, to verify the exogenous expression of human LRRFIP2 or LRRFIP2 mutants in the mouse LRRFIP2 knockdown cells, we enriched the expressed LRRFIP2 or LRRFIP2 mutants through immunoprecipitation by applying equal amounts of FLAG M2-agarose (Sigma-Aldrich) to equal amounts of each transfected cells. The immunoprecipitates were separated on SDS-PAGE and transferred by electroblotting onto nitrocellulose membrane. FLAG-tagged human LRRFIP2 were then detected by using anti-FLAG antibody.

Luciferase Assay—RAW264.7 cells were seeded on 24-well plates 1 day before transfection in 500 μl of growth medium without antibiotics such that they were 60–70% confluent at the time of transfection. Cells were transfected with 100 ng of pGL2-ELAM promoter luciferase transgene and 290 ng of wild-type LRRFIP2, the mutant, or empty vector plasmid, 90 ng of LRRFIP2 shRNA, and 20 ng of pRL-TK as the internal control. An internal control (pRL-TK) that expresses *Renilla* luciferase was co-transfected to normalize the transfection efficiency and sample handling. The cells were exposed to 0.5 μg/ml LPS for 6 h at 24 h after transfection, and the activities of the two different luciferases were assayed with their respective substrates with a Dual-Luciferase assay kit (Promega, Madison, WI). The data were normalized for NF-κB activity, *i.e.* the values obtained from the division of the firefly luciferase activity by the *Renilla* luciferase activity. The results obtained from triplicate runs of each sample were then averaged. The data presented are the mean ± S.E. (n = 3). Similar results were obtained in three independent experiments.

Co-immunoprecipitation and Immunoblotting—293T cells stably expressing TLR4-MD2 (stable cells) were transiently transfected with HA-MyD88 and either wild-type FLAG-LRRFIP2 or FLAG-LRRFIP2 mutants such as S202A, S202E, etc., respectively. The cells were treated with 1 mg/ml LPS and harvested at different time points after the LPS stimulation. The cells were lysed with lysis buffer (1% Nonidet P-40, 50 mM Tris-HCl (pH 7.6), 150 mM NaCl, 2 mM EDTA, 1 mM sodium vanadate, 5 μg/ml leupeptin, 5 μg/ml aprotinin, and 1 mM PMSF), and precleared by centrifugation at 16,000 × g for 15 min. About 1 mg of total protein was incubated with or without the indicated antibodies for 1 h at 4 °C and subsequently with protein A- or protein G-agarose beads overnight at 4 °C on a rotating platform. After centrifugation, beads were washed five times with lysis buffer. Bound proteins were eluted with the SDS sample buffer.

The immunoprecipitation and whole-cell lysate samples were separated on a 3–8% Tris acetate gel (Invitrogen) and transferred to nitrocellulose membrane, and the membrane was then blocked with 5% milk in 1× Tris-buffered saline with 0.01% Tween 20 (1× TBS-T). The membrane was then incubated with the appropriate primary antibodies for 4–6 h, washed five times with 1× TBS-T, and then incubated with the appropriate HRP-linked secondary antibodies for 1 h. The membrane was again washed five times with 1× TBS-T, incubated with chemiluminescent substrate for 1 min, and then exposed to film and visualized using the ECL Plus detection system (GE Healthcare).

RESULTS AND DISCUSSION

MS-based Label-free Quantitation—Using anti-FLAG antibody, we took a snapshot of FLAG-tagged LRRFIP2 by immunoprecipitating it from TLR4 stable HEK cells at 0, 2, 5, 10, 20, and 60 min after LPS stimulation. To compare the ratio of phosphorylated to nonphosphorylated peptide ions, tryptic digests of LRRFIP2 isolated at each time point were separated by high-resolution liquid chromatography, and all LRRFIP2-specific phosphopeptides were analyzed by mass spectrometry. Full-scan MS was performed on the accurate mass, high-resolution Orbitrap mass analyzer for precise mass measurement of peptide precursor ions and XIC. Quantitation was performed on the XIC corresponding to the LC elution profile of the peptide

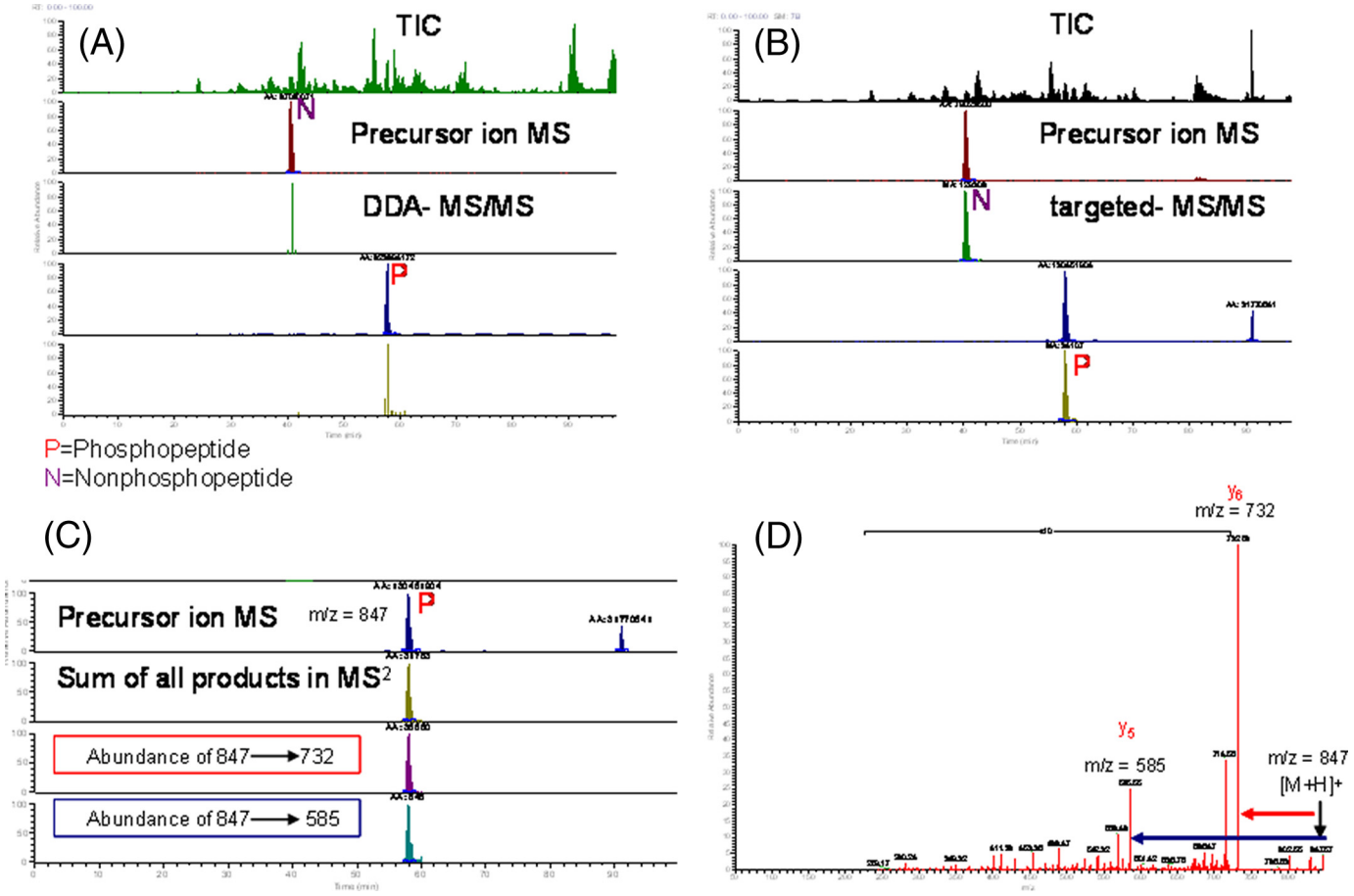

FIGURE 1. **Label-free quantitation of a phosphopeptide and corresponding nonphosphopeptide counterpart in a single LC-MS/MS run.** *A*, XIC of precursor ions derived from data-dependent analysis (*DDA*)-MS/MS. *B*, XIC of product ions derived from a targeted CAD-MS/MS. *C*, reconstructed SRM profile using specific precursor-product ion pairs of phosphopeptide P. *D*, CAD-MS/MS of the corresponding phosphopeptide P.

of interest. Quantitation of LPS-induced changes for each phosphopeptide and its nonphosphorylated counterpart was carried out by aligning the retention times of the XIC profiles, verifying the peptide identity, and unambiguously identifying sites of phosphorylation based on the MS/MS spectrum.

Fig. 1 illustrates the complementary nature of the intensity-dependent, targeted label-free, and single-reaction monitoring (SRM) approaches used for quantitation of phosphopeptides. The intensity-dependent MS/MS approach uses the full-MS spectrum ion count for a peptide of interest to derive the chromatographic peak profile of the eluting peptide (Fig. 1*A*). However, the number of data points obtained in MS/MS was insufficient (<7 for a 30-s peak width) to reconstruct the elution profile for quantitation purposes. The targeted approach relies on confident identification of phosphopeptides and corresponding nonphosphopeptides, which are subsequently mapped to the amino acid sequence of the intact protein (Fig. 1*B*). The mapping accounts for phosphopeptides with overlapping sequences, other modifications, and adducts that constitute a phosphorylation site. Most often, intensity/data-dependent acquisition methods do not trigger MS/MS fragmentation for every charge state, adduct, or modification and, hence, do not enable the identification of every peptide species. To circumvent this issue, we combined an MS^3 approach (see supplemental Fig. 1S) to identify phosphopeptides with targeted MS/MS experiments using MS/MS spectrum ion counts to reconstruct the elution profile for quantitation. The SRM approach uses specific precursor-product ion transitions from a MS/MS spectrum to reconstruct the elution profile of the peptide of interest for quantitation (Fig. 1*C*). SRM experiments performed on an Orbitrap mass spectrometer are analogous to SRM experiments conducted on a triple quadrupole instrument (42). The SRM experiment itself can be carried out in the Fourier transform/ion trap (FT/IT) mode in which precursor detection is based on Orbitrap (FT) mass measurement followed by dissociation and product mass analysis in the linear IT. For greater specificity, SRM data can be collected in the FT/FT mode, in which both the initial precursor and ensuing dissociation products are detected in the Orbitrap (FT). Although the targeted SRM approach improves the specificity, it does so at the cost of sensitivity, as evidenced by a reduction in the ion count. To our knowledge, this is the first report of both qualitative and quantitative peptide information obtained from data-dependent MS/MS in conjunction with Orbitrap SRM performed on a single instrument.

Using this array of complementary techniques, we identified 23 specific phosphorylation sites among a total of 34 LRRFIP2 phosphopeptides. In addition, we measured and quantified LPS-induced temporal changes in 11 LRRFIP2 phosphorylation sites. Here, we present quantitation data for selected LRRFIP2

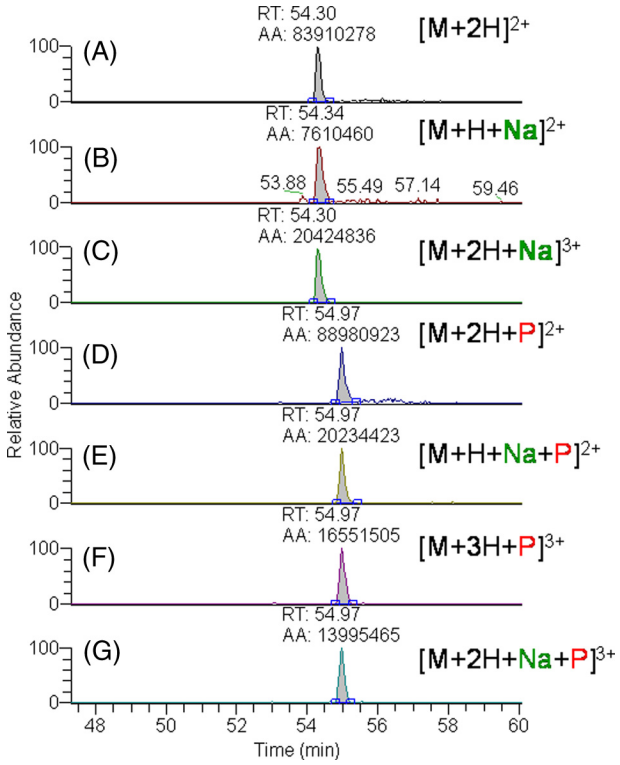

FIGURE 2. **XIC of a doubly and triply charged peptide of *M* = S^{200}AS^{202}LASLYNGGLYNPYGR.** *A–C*, nonphosphopeptide. *D–G*, phosphopeptide. *P*, phosphorylation; *Na*, sodiation.

peptides (SASLASLYNGGLYNPYGR, RGSGSDTSSLIDPDTSLSELR, SDRASPATANGGLR, and ASPATANGGLR) to illustrate the utility of label-free approaches for determining statistically significant changes in phosphorylation upon LPS stimulation. The biological function associated with each of the newly identified phosphorylation sites is under investigation and will be reported elsewhere.

Comprehensive Label-free Quantitation of LPS-induced Dynamics of Multiple LRRFIP2 Phosphopeptides—Fig. 2 shows the XIC profiles of the SASLASLYNGGLYNPYGR peptide species observed in a single LC-MS run. Both phosphorylated and nonphosphorylated SASLASLYNGGLYNPYGR peptide subpopulations are present in a given sample. In addition, metal ion adducts (*e.g.* from sodium), shifts in charge state distribution, and modifications (*e.g.* deamidation of asparagine residues) could exist within each subpopulation and contribute to the total ion signal. From the standpoint of label-free quantitation methods based on the consideration of peak area, all of these subpopulations must be taken into account to avoid quantitative inaccuracies due to sample-to-sample variability.

Degenerate charge states and adducts are a consequence of the electrospray ionization process, whereas deamidation is an experimental artifact introduced during sample handling. The mass and charge degeneracy introduced for the SASLASLYNGGLYNPYGR peptide in our experiments was mainly due to 3+ and 2+ charge states, sodium adduction, and deamidation of asparagine. The mass difference between charge states and sodium adduct peaks is typically large enough to distinguish the peak area of each component based on the XIC. However, deamidation of asparagine to isoaspartic acid results in a mass shift of 0.987 Da for an ion of 1+ charge, 0.4 Da for a 2+ ion, and 0.3 Da for a 3+ ion. The isotope clusters of the deamidated and nondeamidated multiply charged peptides cannot be chromatographically resolved and are therefore irrelevant for use in peak area calculations based on XICs. Because deamidation of the SASLASLYNGGLYNPYGR peptide has no biological relevance, peak areas corresponding to both the deamidated and nondeamidated forms were simply summed in our calculations.

In the case of some LRRFIP2 peptides sharing common sequences, such as SD**R**ASPTANGLLR and ASPATANGGLR, in which the longer peptide results from a single missed tryptic cleavage (underlined in bold), the phosphorylation pattern of each peptide may be similar or different and mutually exclusive. The quantitative approach taken to determine the phosphorylation state of a peptide depends on the localization of the phosphorylation site; this will be described in greater detail below. For example, if the identified phosphorylation site is similar for two degenerate peptides, quantitation is achieved by summing the peak areas of the degenerate forms. However, if the phosphorylation site is different in each peptide, each is considered as an independent phosphorylation site, and quantitation cannot be achieved by summing the peak areas.

Equation 1 was used to quantitate LPS-induced temporal changes in the phosphorylation of three LRRFIP2 phosphopeptides. As shown in Fig. 3, most of the change in the abundance of the phosphorylated forms occurred within 10 min of LPS stimulation. The abundance of the SASLASLYNGGLYNPYGR phosphopeptide increased by ~2-fold, whereas the RGSGSDTSSLIDPDTSLSELR, SDRASPATANGGLR, and ASPATANGGLR (combined is denoted as *SDR*ASPTANGGLR) peptides exhibited a 0.8–1.5-fold increase in phosphorylation over the same time period. Fig. 3, *inset 2*, shows an overlay of XICs for both the SASLASLYNGGLYNPYGR phosphopeptides (*P*) and nonphosphopeptides (*N*) at selected time points. Similarly, no other LRRFIP2 phosphopeptides exhibited a quantitative phosphorylation fold-change greater than 2 (minimum of three biological replicates over the time course). On the basis of this observation and the fact that the majority of phosphorylation sites showed very little to no change following LPS stimulation, we set a 2-fold increase as the threshold for a statistically significant change in phosphorylation. It is conceivable that a quantitative change of less than 2-fold may also be biologically significant in specific instances, as demonstrated previously by quantitative mass spectrometry (12).

Cross-method Comparison of Quantitative Accuracy Provided by the AACT/SILAC-based versus Label-free Quantitative Approaches—We further adapted the 3-plex AACT-based quantitation approach (23), which was performed independently from the label-free approaches with selected time points to verify the accuracy of our label-free quantitation data. The cross-method comparison/verification of site-specific phosphorylations identified by using multiple quantitative methods gives additional confidence in the accuracy of our newly developed methods to screen physiologically relevant phosphorylation sites. Fig. 4 shows precursor ion pairs of the unlabeled and Leu-d_3-labeled phosphopeptides SASLASLYNGGLYNPYGR, SDRASPATANGGLR, and ASPATANGGLR and a few non-

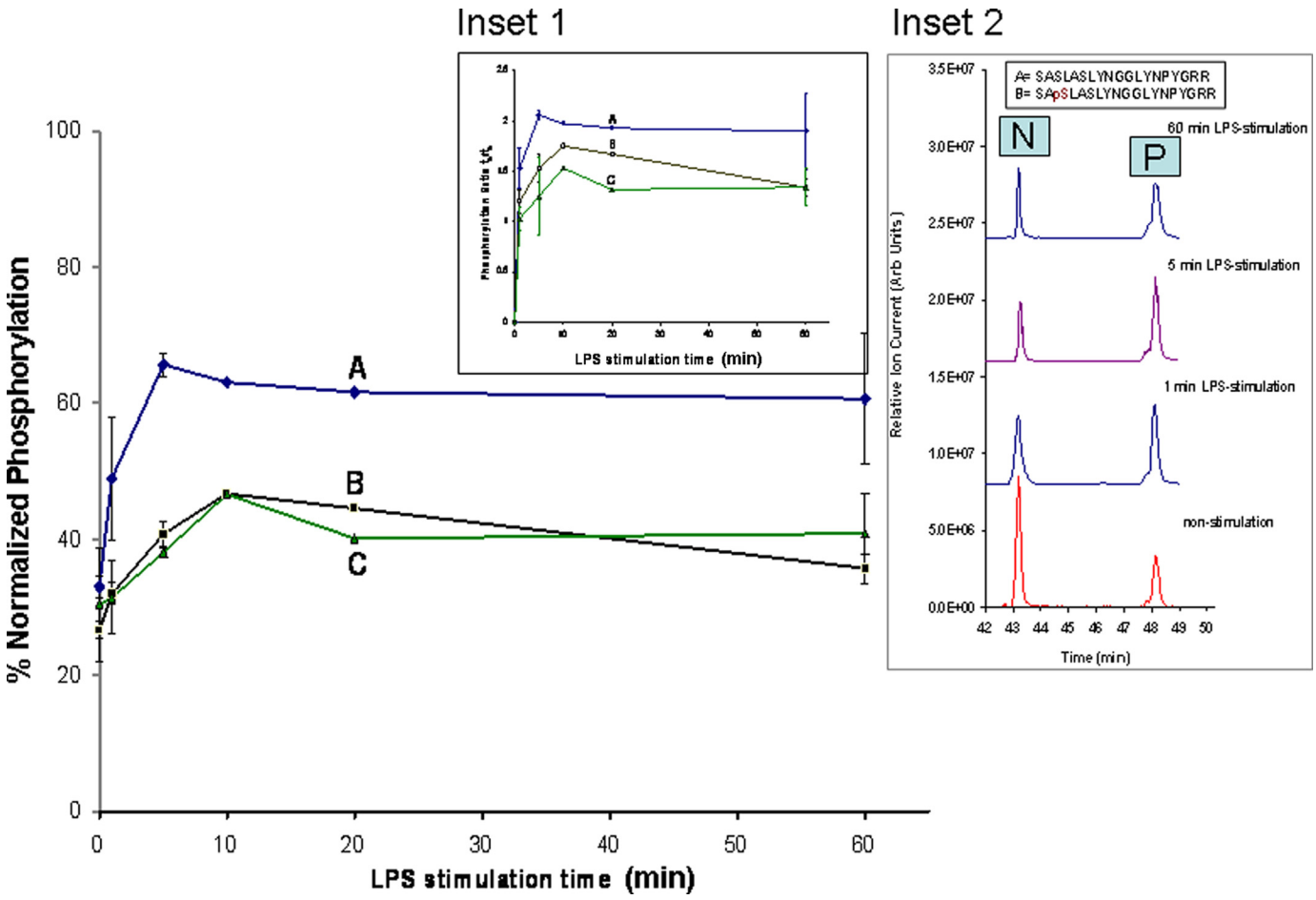

FIGURE 3. **LPS-induced phosphorylation dynamics of selected LRRFIP2 peptides: SASLASLYNGGLYNPYGR (*A*), ASPATANGGLR (*B*), and RGSSVVSEVD-DISIPDLSSLDEK (*C*).** *Inset 1* shows -fold changes with respect to nonstimulated $t = 0$ min. *Inset 2* shows the XIC of *A* over the selected time points, where phosphopeptide and corresponding nonphosphopeptide peaks are shown as *P* and *N*, respectively.

phosphopeptides of LRRFIP2. The SILAC ratio for each peptide is obtained by computing the peak area ratio of the isotope clusters between nonstimulated and LPS-stimulated conditions. The raw MS spectrum of the precursor ion of the SASLASLYNGGLYNPYGR phosphopeptide shows a significantly higher SILAC ratio of 2.1 compared with other phosphopeptides and nonphosphopeptides of LRRFP2. For example, the corresponding average SILAC ratio of 16 leucine-containing nonphosphorylated LRRFIP2 peptides was 1.15 ± 0.1, whereas for nine leucine-containing phosphorylated peptides it was 1.18 ± 0.1 (data not shown). The SILAC ratio of the nonphosphorylated peptides was normalized based on LRRFIP2 nonphosphopeptide ratios that remained static. The normalized SILAC ratios are in close agreement with the label-free data for most of the commonly detectable phosphopeptide including the SASLASLYNGGLYNPYGR peptide (see supplemental Fig. 2S). Meanwhile, a larger number of LRRFIP2 phosphopeptides were quantified via label-free (11 peptides) compared with (seven peptides) SILAC quantitation, suggesting high sequence coverage of the label-free quantitation method for analyzing the LPS-induced dynamics of multiple phosphopeptides of an individual protein.

Discovery-based Precise Localization of Phosphorylation Sites for Streamlined Biological Characterization—Unambiguous assignment of phosphorylated residues in peptides with multiple potential phosphorylation sites is a critical step in streamlining concurrent biological experiments. There are several approaches for localizing *a priori* unknown phosphorylation sites. Unambiguous localization of modifications is conventionally carried out by matching to a spectral library of standard peptides. However, when spectra are unavailable, phosphopeptide synthesis is impractical for mid-to-large-scale data sets. We performed complementary ion dissociation methods such as CAD and ETD to obtain spectra for subsequent interpretation both manually and with automated protein database search algorithms. Phosphosite localization software was then used to verify the experimentally identified phosphorylation sites. Using this novel combination of methods, we have demonstrated the data-dependent assignment of site-specific phosphorylation for two representative phosphopeptides, SASLASLYNGGLYNPYGR and SDRASPTANGLLR from LRRFIP2, in which the phosphorylation level changed 2- and 1.5-fold, respectively, 5 min after LPS stimulation.

The CAD product ion spectrum of the doubly protonated phosphopeptide SASLASLYNGGLYNPYGR (Fig. 5*A*) is comprised of *b*- and *y*-type fragment ions resulting from peptide backbone cleavages and a predominant neutral phosphoric acid loss peak due to β-elimination of a phosphate-containing side chain. The loss of phosphoric acid (H_3PO_4) is characteristic of both phosphoserine- and phosphothreonine-containing pep-

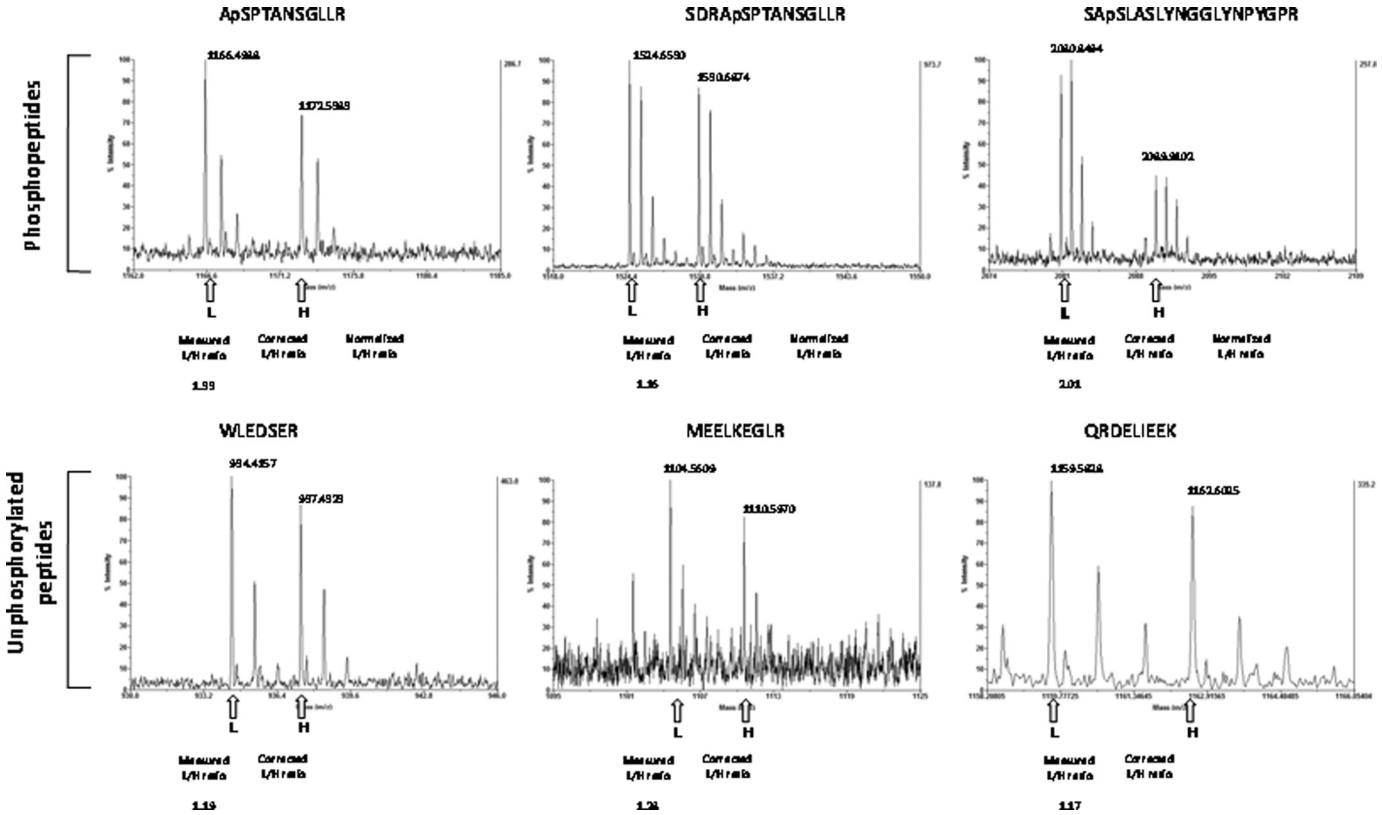

FIGURE 4. **AACT/SILAC-based quantitation of LRRFIP2 phosphopeptides ASPTANSGLLR, SDRASPTANSGLLR, and SASLASLYNGGLYNPYGR and LRRFIP2 protein ratios of selected nonphosphopeptides with the measured and normalized peptide ratios.**

tides and can therefore be used to prescreen phosphopeptides. However, the facile loss of phosphoric acid often leads to both low abundance backbone fragments and fragments lacking the phosphate moiety. Localization of a phosphorylation site in CAD-MS/MS spectra is often challenging when several potential phosphorylation sites are present on a single peptide, as is the case with SASLASLYNGGLYNPYGR and SDRASPTANGLLR. We therefore used a neutral phosphoric acid loss MS^3 experiment to identify the phosphorylation sites in these peptides (see supplemental Fig. 1S). The CAD-MS/MS product ion spectrum of the SASLASLYNGGLYNPYGR peptide consists of both *b*- and *y*-type ions, of which nearly all of the *b*-type ions (*b*8 + P, *b*13 + P, *b*14 + P, and *b*15 + P) (See Fig. 5*A*) contain a phosphate moiety, suggesting that the phosphorylation site may be on Ser-1, Ser-3, Ser-6, or Tyr-8. The only *b*8 fragment ion observed in the spectrum presumably results from H_3PO_4 loss, as only *y*8 + P/*y*11 complementary ion pairs were observed. The lack of a contiguous *b*-type ion series limits the ability to localize the phosphorylation site using complementary *y*-type ions. With the exception of a single product ion (*y*17 + P), all of the *y*-type ions lacked a phosphate moiety (*y*5, *y*6, *y*7, *y*10, *y*11, *y*12, *y*13, *y*14, *y*15, *y*16, and *y*17 + P) (See Fig. 5*A*). The *b*8 + P and *y*17 + P ions suggest that Ser-3, Ser-6, or Tyr-8 is phosphorylated, whereas the presence of *y*16 but not *y*16 + P suggests that Ser-1 should also be considered as a potential phosphorylation site.

The Mascot search results shown in Table 1 list all of the possible phosphorylation sites along with their respective ion scores, which is helpful in localizing the correct phosphorylation site via manual interpretation efforts. The highest ion score is shared by potential phosphorylations on residues Ser-1 and Ser-3. The Mascot scoring algorithm is based on all the fragment ions, including fragment ions that do not contain a phosphate moiety. This type of scoring becomes problematic for phosphopeptides and may lead to ambiguous assignments with multiple possibilities, as most phosphate-loss ions are included in the scoring.

The *y*16 fragment ion maybe a second generation neutral loss peak and is therefore too ambiguous to assign Ser-1 as a phosphosite. Similarly, the *y*11–*y*15 ions may be second generation product ions resulting from the loss of phosphoric acid. If the assignment was based exclusively on phosphate-containing sequence ions, the phosphorylation could be assigned to Ser-3, Ser-6, or Tyr-8. Residues Ser-3 and Ser-6 are the most likely candidates because of the dominant H_3PO_4 (98 Da) loss peak common to phosphoserine-containing peptides. However, phosphotyrosine-containing peptides usually produce a HPO_3 (80 Da) neutral loss along with a sequential loss of H_2O (18 Da), which makes its neutral loss product ions analogous to a H_3PO_4 loss.

In addition to Mascot scoring and manual verification, we also used the Ascore (ambiguity score) program to assist in confidently localizing the site of phosphorylation (31). The Ascore algorithm is a probabilistic method for assigning phosphorylation sites within a given phosphopeptide. The program uses Sequest search results and spectral data as inputs to detect phosphospecific fragment ions. The Ascore values obtained for the SASLASLYNGGLYNPYGR peptide are shown in Table 1

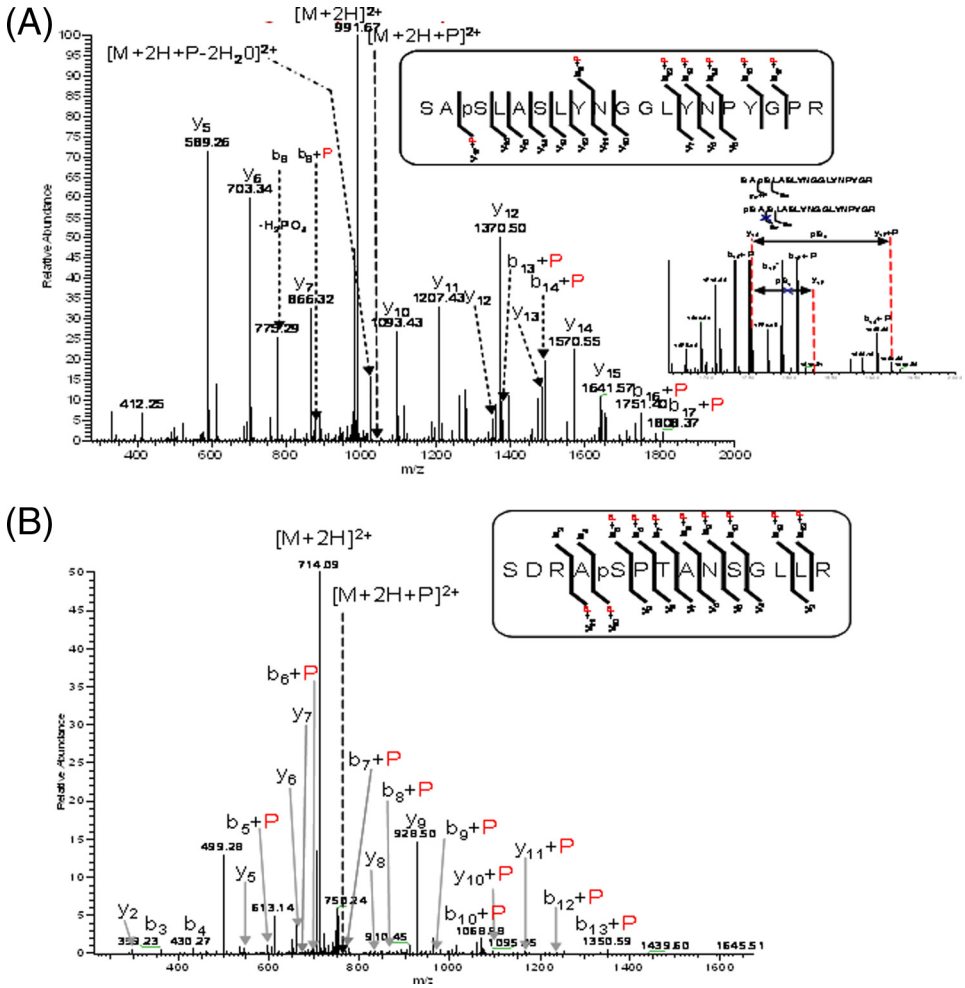

FIGURE 5. **Product ion spectra resulting from CAD-MS/MS of doubly protonated phosphopeptides SASLASLYNGGLYNPYGR (*A*) and SDRASPATANGGLR (*B*).**

TABLE 1

Identification and localization of LRRFIP2 phosphorylation sites

Mascot ion scores are significant for identity threshold > 32 and homology threshold > 22. Ascore > 19 ($p = 0.01$); 19 > Ascore > 15 ($p = 0.1$) and 15 > Ascore > 5 ($p \sim 0.8$). Proton mobility: mobile proton peptides, number of protons > number of arginine residues; nonmobile proton peptides, number of protons ≤ number of arginine residues.

LRRFIP2 sequence	Residues	Mascot ion score (Mascot % confidence)	Ascore	Phospho-site (Ascore % confidence)	Proton mobility for Z = +2
SASLASLYNGGLYNPYGPR	200–218	88 (99)		Ser-200	Mobile
		88 (99)	16	Ser-202 (>90)	
		59 (99)	11.01	Ser-205 (~80)	
		35 (95)	4.35	Tyr-207	
RGSGDTSSLIDPDTSLSELR	326–345	112 (99)	61.52	Ser-328 (>99)	Non-mobile
ASPTANSGLLR	186–199		48.59	Ser-190 (>99)	Mobile
SDRASPTANSGLLR	189–199	48 (99)	28.76	Ser-190 (>99)	Non-mobile

and were used to determine the confidence associated with assigning a particular residue as the site of phosphorylation. Residue Ser-3 (LRRFIP2 residue Ser-202) had the highest score (>90% confidence) followed by Ser-6 (LRRFIP2 residue Ser-205) and Tyr-8 (LRRFIP2 residue Tyr-207) with ~80% confidence. The Ascore values do not unambiguously localize the phosphorylation site within the SASLASLYNGGLYNPYGR peptide based on CAD data. The ambiguity associated with localizing phosphorylation sites using Ascore is due to the absence of phosphate-containing sequence ions that can distinguish each site. Incorrect assignment due to either a gas phase rearrangement of the phosphate group or the presence of isomers necessitates further analysis when multiple potential phosphorylation sites are present on a peptide. Therefore, we used motif-x to predict possible phosphorylation motifs on LRRFIP2 peptides along with the program Scansite to identify the residue-specific kinases involved in the phosphorylation (31). Data from these analyses narrowed the potential targets of phosphorylation to residues Ser-3 and Ser-6.

Further, to distinguish those "artificial" phosphorylations that could occur in gas phase under nonphysiological conditions, we also looked at the propensity for the same peptide

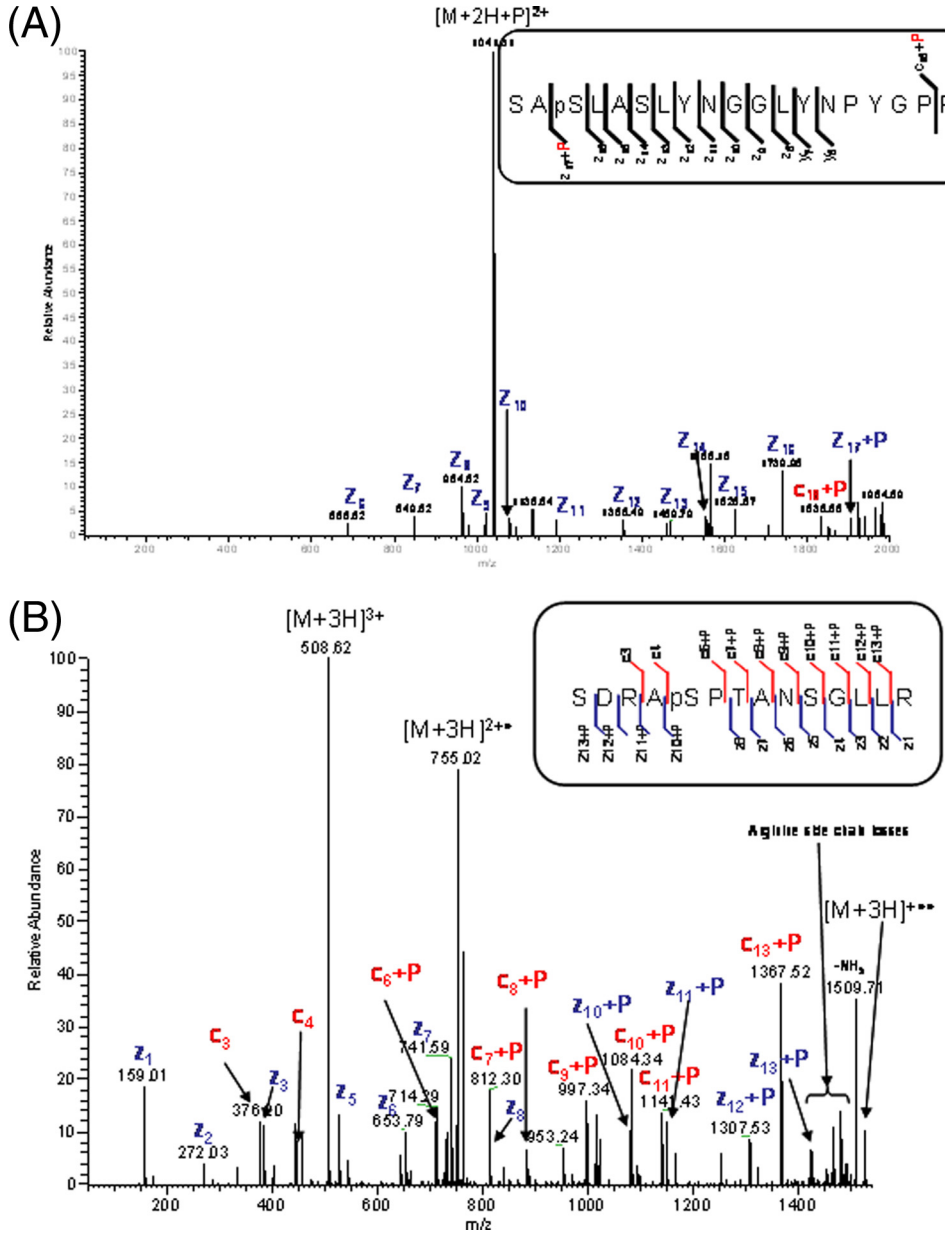

FIGURE 6. **Product ion spectra resulting from ETD-MS/MS of protonated phosphopeptides SASLASLYNGGLYNPYGR (*A*) and SDRASPATANGGLR (*B*).**

sequence to undergo phosphate group transfer reactions under various charge state and protonation conditions (see supplemental Fig. 3S). The SASLASLYNGGLYNPYGR peptide satisfies the conditions for having mobile protons; that is, the number of protons on the peptide is greater than the number of arginine residues (33). It is therefore less likely that a phosphate group transfer would occur in this peptide during CAD. However, when the same peptide having a sodium ion substituted for a proton was subjected to CAD-MS/MS, the product ions were significantly different than those of the fully protonated analog. The most dominant fragment ion was a neutral H_3PO_4 loss, which is typically observed in peptides that have non-mobile protons. Manual analysis of the product ions identified Ser-1 as the phosphorylation site, presumably because of rearrangement of the phosphate group. To confirm this prediction, we subjected a doubly protonated SASLASLYNGGLYNPYGR peptide to ETD-MS/MS. The ETD technique preserves labile post-translational modifications such as phosphorylation while cleaving peptide N–Cα bonds to yield *c*- and $^{\bullet}$*z*-type fragment ions. Fig. 6*A* shows the ETD-MS/MS product ion spectrum resulting from the ion/ion reaction of the doubly protonated SASLASLYNGGLYNPYGR peptide. A contiguous $^{\bullet}$*z*-type product ion series (*z*6–*z*17 + P) along with a single *c*-type product ion (*c*18 + P) was observed. The charge-reduced and undissociated singly charged product ions were not within the detectable *m*/*z* and therefore were not observed. The almost exclusive presence of *z*-type ions was expected due to the retention of charge on the arginine residue. The *z*17 + P and *z*16 product ions allowed us to confidently assign Ser-3 (LRRFIP2 residue Ser-202) as the single phosphorylation site on SASLASLYNGGLYNPYGR.

Fig. 5*B* shows the CAD product ion spectrum of the SDRASPTANGLLR peptide, which consists of the contiguous series $b5 + P - b13 + P$ and $y11 + P - y10 + P$. Based on this spectrum, the phosphorylation site was unambiguously localized to Ser-5. In addition, CID fragmentation of the ASPTANGLLR peptide also confidently localized the phosphate group to Ser-5 (LRRFIP2 residue Ser-190). The Ascore for both the ASPTANSGLLR and SDRASPTANSGLLR peptides indicated that the phosphorylation site was on Ser-2 and Ser-5, respectively (both corresponding to LRRFIP2 residue Ser-190), with >99% confidence.

An ETD-MS/MS spectrum of the triply protonated SDRASPTANSGLLR peptide (shown in Fig. 6*B*) was also obtained to localize the phosphorylation site(s). The presence of a contiguous series of phosphate containing *c*-type ions ($c6 + P - c13 + P$) along with their corresponding complementary $^{\bullet}z$-type ions ($z1$–$z8$) suggests that the phosphorylation site may be either Ser-1 or Ser-5. The contiguous series of phosphate containing *z*-type ion series ($z10 + P - z13 + P$) with complementary *c*-type ions ($c3$ and $c4$) suggests that the site of phosphorylation is Ser-5, Thr-7, or Ser-10. However, when both *c*- and $^{\bullet}z$-type phosphate-containing product ions are considered, the phosphorylation site could be unambiguously localized to within two residues of Ser-5 (serine 190 at LRRFIP2). The lack of N-terminal proline cleavage during ETD fragmentation complemented by a dominant N-terminal proline cleavage during CAD fragmentation localizes the site of phosphorylation to within a single residue of Ser-5.

Characterization of the Functional Role of LPS-inducible Phosphorylation in TLR4 Signaling—The biological characterization experiments were performed on identified phosphorylation sites showing LPS-inducible changes either greater than or less than the 2-fold threshold. These experiments provide a means of evaluating the biological accuracy of LPS-induced site-specific phosphorylation changes determined by label-free quantitation and also illustrate the biological significance/relevance of our quantitative threshold. Specifically, we explored the possible impact of certain newly identified phosphorylation sites on the LPS-induced interaction between LRRFIP2 and MyD88, which in turn may affect downstream NF-κB activity.

We have focused on three serine residues, Ser-190, Ser-200, and Ser-202, which represent three different categories of the phosphorylation quantified and identified by our label-free approach. Ser-190 showed a 1.5-fold increase in its phosphorylated form in early cellular response to LPS (Fig. 3), whereas an LPS-induced 2.0-fold increase in phosphorylation was observed for the peptide consisting of Ser-200 and Ser-202. The unambiguous identification of phosphorylation at Ser-202 and the false-positive identification of phosphorylation at Ser-200 due to a gas phase relocation of the phosphate group (supplemental Fig. 3S) therefore suggested that the 2-fold change was solely attributable to Ser-202, whereas Ser-200 remained completely devoid of phosphorylation, at least under these conditions. We could therefore assign Ser-200 as a negative control for all biological experiments, whereas the Ser-190 and Ser-202 sites having different phosphorylation fold changes were evaluated for their biological activity.

Through site-directed mutagenesis, we substituted each of the serine residues at positions 190, 200, and 202 or their combination with alanine or glutamic acid to make the phosphorylation-depleted single or double mutants. These mutants include S202A, S202E, S200A, S190A, and S202A,S190A, respectively. Conversely, the S202E mutant was made to mimic the charge state of the phosphorylated LRRFIP2 at Ser-202.

First, the effect of site-specific phosphorylation or "lack thereof" on LPS-induced signal transduction was assessed by comparing both differences in NF-κB activity associated with human wild-type LRRFIP2 *versus* the corresponding mutants. By using shRNA (12) we first knocked down the endogenous mouse LRRFIP2 in RAW cells and then transfected RAW cells with the human version of either wild-type LRRFIP2 or each of these mutants by using a relatively efficient jetPRIME transfection kit. Fig. 7*A* shows that we achieved a 60% knockdown of endogenous mouse LRRFIP2 compared with scrambled shRNA. Because of the low abundance of LRRFIP2 in total cell lysates, the expression of each exogenous human LRRFIP2 or its mutant transfected into RAW cells was measured by immunoblotting following an enrichment step of immunoprecipitation on the equal amount of each transfected cells with equal amount of anti-FLAG beads (Fig. 7*B*). LPS-induced NF-κB activity was then determined via a luciferase reporter assay on the RAW macrophage cells transfected with the human version of either wild-type LRRFIP2 or each of these mutants, respectively. As a result, although the mutants, S190A, S200A, and S202E, did not show any measurable change in NF-κB activity compared with the wild-type LRRFIP2, we found that the abolishment of the phosphorylation propensity at Ser-202 (*i.e.* S202A) led to a 44% reduction of LPS-induced NF-κB activity (Fig. 7*C*). Similar to the S202A mutant, the macrophages transfected with the double mutant S202A,S190A showed a 43% reduction in NF-κB activity, implying that the reduction in NF-κB activation is primarily attributable to the depletion of serine at position 202, and the loss of phosphate at serine 190 has little effect on NF-κB activity. We also comparatively measured the changes in NF-κB activity caused by the direct transfection of either the wild type or each LRRFIP2 mutant to the RAW cells without pre-LRRFIP2 knockdown by shRNA. An approximate 20% reduction in NF-κB activity was observed (supplemental Fig. 4S), indicating that the actual effect of the phosphoserine at 202 on NF-κB activity is undermined by endogenous wild-type LRRFIP2. Considering that the endogenous wild-type LRRFIP2 residual in RAW cells may contribute to the overall LPS-induced NF-κB activity, the actual effect of the LPS-inducible phosphorylation at Ser-202 on NF-κB activity in the cells with a complete wild-type "knock-out" should be more than the observed 44% reduction.

Further, because of the regulatory role of dynamic MyD88-LRRFIP2 interaction in modulating downstream LPS-induced NF-κB activity, we comparatively examined the LPS-induced and time course-dependent binding between MyD88 and either wild-type LRRFIP2 or the S202A or S202E LRRFIP2 mutant, respectively, across the full course of LPS-induced TLR4 signaling. We transiently co-transfected HA-tagged MyD88 with FLAG-tagged LRRFIP2 or the S202A or S202E mutant, respectively, along with MD2 to the HEK293T cells

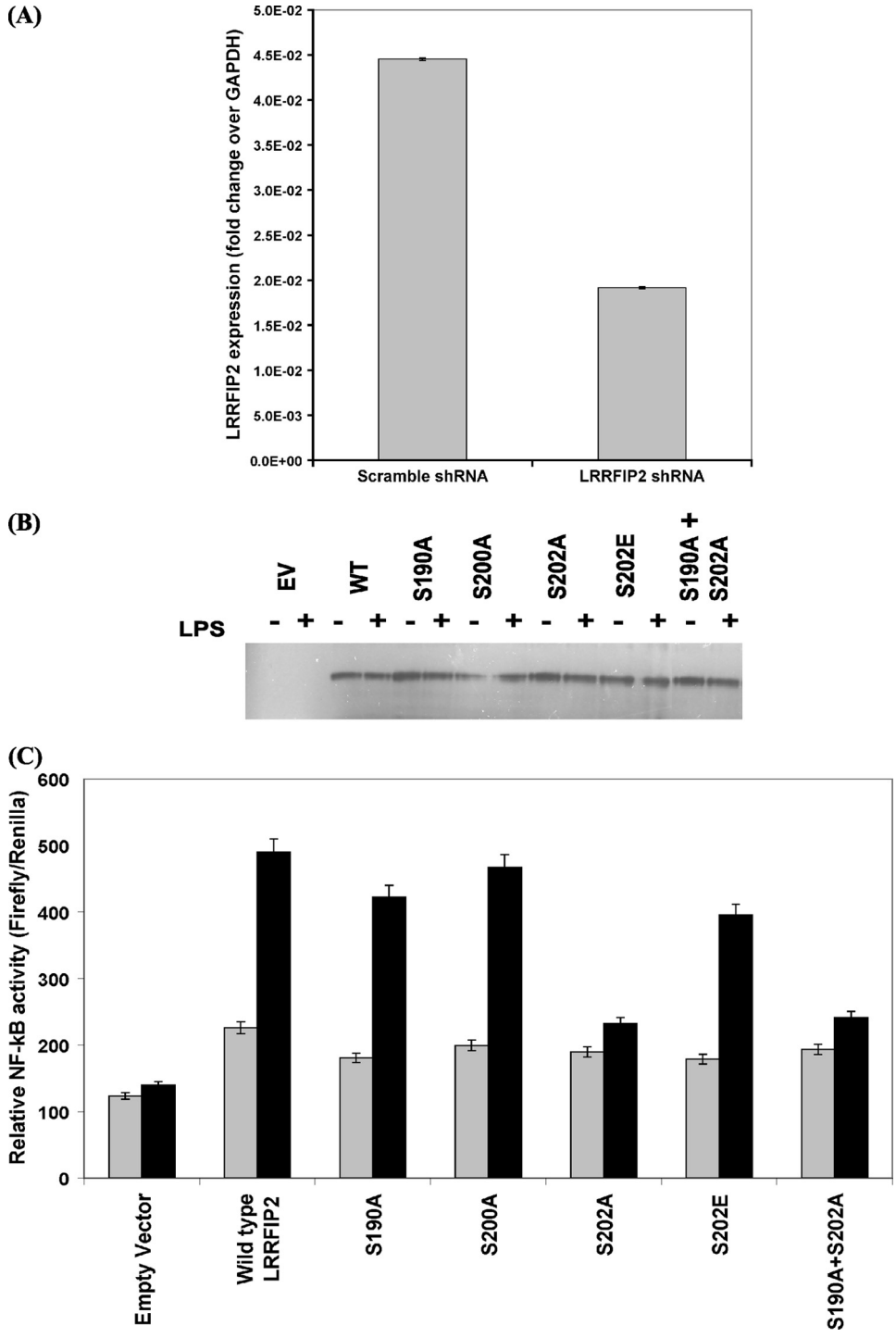

FIGURE 7. *A*, close to 60% knockdown of endogenous mouse LRRFIP2 was found in RAW264.7 cells using shRNA. Scrambled shRNA was used as a negative control. *B*, expression of human LRRFIP2 constructs in the endogenous mouse LRRFIP2 knockdown background in RAW264.7 cells. Cells were transfected with each construct and lysed, and the protein was immunoprecipitated using the FLAG tag. *EV*, empty vector. *C*, NF-κB activity of the human LRRFIP2 mutants in RAW264.7 cells in the background of mouse LRRFIP2 knockdown.

stably expressing TLR4 and then stimulated these cells with LPS. The LPS-stimulated cells were collected, respectively, at different time points (0, 5, 10, 15, 20, 30, 60, and 120 min), and the MyD88-interacting complex was pulled down using the HA tag. The population of the MyD88-associating LRRFIP2 or its mutants was detected by immunoblotting using anti-FLAG antibody. In the immunoprecipitate isolated from unstimulated resting cells, two bands in doublet were observed for the MyD88-LRRFIP2 association at a basal level (Fig. 8, *top panel*). In the complexes pulled down from the stimulated cells following LPS stimulation for 5–15 min, the intensity of this doublet indicative of the binding strength between MyD88 and wild-type LRRFIP2 was significantly enhanced along with a newly appearing slow-migrating species. A longer LPS stimulation for 20–30 min resulted in decreased binding between LRRFIP2 and MyD88, implicating possible dissociation of LRRFIP2 from

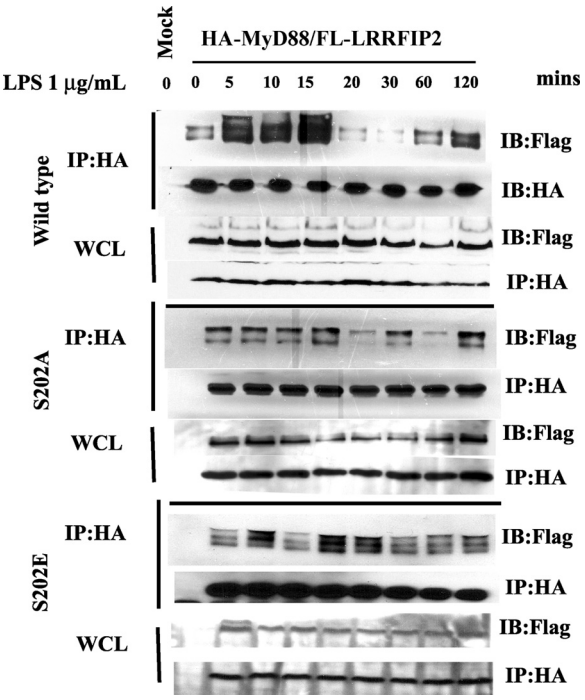

FIGURE 8. **Changes in the interaction between wild-type LRRFIP2 and MyD88 upon LPS stimulation.** Cells were transfected for transient expression of wild-type FLAG-LRRFIP2 or its mutant S202A or S202E, HA-MyD88, and MD2 as described under "Experimental Procedures." Mock control was not transfected with plasmid DNA. Cells were then stimulated with or without LPS at 1 μg/ml for various amounts of time as indicated. Cells were lysed, and the MyD88-interacting complex was immunoprecipitated. Whole-cell lysates (*WCL*) and immunoprecipitates (*IP*) were analyzed by Immunoblotting (*IB*) for FLAG-LRRFIP2 and HA-MyD88.

the MyD88 complex. LPS stimulation for 60–120 min resulted in a slight increase in their interaction; however, it was comparatively less than the interaction during the onset between 5–15 min of LPS-induced interactions. Furthermore, after 20 min of LPS stimulation, the migration pattern associated with the increased levels of phosphorylated LRRFIP2 reverted back to the doublet pattern observed for unstimulated cells. Overall, these LPS-induced changes in the MyD88-LRRFIP2 binding pattern closely correlate with the dynamic changes in LRRFIP2 phosphorylation, as evidenced by our label-free quantitative mass spectrometry results (Fig. 3). In contrast, MyD88 binding to the LRRFIP2 S202A mutant showed only two species, which were apparently not LPS-inducible and remained little changed through the full course following LPS stimulation (Fig. 8, *middle panel*). Further, in the binding of MyD88 to LRRFIP2 S202E, the slow-migrating species, which appeared only after 5 min of LPS stimulation in the cells transfected with wild-type LRRFIP2 (Fig. 8, *top panel*), was observed under the unstimulated state (Fig. 8, *bottom panel*), implying that the slow-migrating species mimicked by a glutamic acid corresponds to the LPS-induced phosphorylation of LRRFIP2 at Ser-202. Further, although this binding pattern was shown to differ from that of MyD88 with wild-type LRRFIP2, the interaction between MyD88 and the LRRFIP2 S202E mutant is clearly LPS-inducible with enhanced binding during the first 20 min. All of these observations firmly indicated that the addition of a net negative charge to LRRFIP2 by either phosphate group or phosphomimetic glutamic acid is essential for the signal-promoting interaction between MyD88 and LRRFIP2. In correlation with the mutation effect on NF-κB activity, our results collectively indicated that site-specific phosphorylation at LRRFIP2 is indeed involved in regulating the interaction between LRRFIP2 and MyD88 to modulate the dynamics of NF-κB regulation upon LPS stimulation.

Here, our study provides clear evidence of how an LPS-inducible dynamic and site-specific phosphorylation at the signal protein, LRRFIP2, could regulate its temporal interaction with the critical TLR adaptor protein MyD88, which controls TLR4-mediated cellular signaling in a timely and orderly manner. Using our targeted MS-based label-free quantitation approach, both precise quantitation and unambiguous identification can be achieved for site-specific phosphorylation, with clear implications for their possible functional role in signal transduction. This multiplex quantitation methodology uses both phosphopeptide and nonphosphopeptide counterparts for relative quantitation across various time points during the full course of the cellular response to LPS stimulation. To our knowledge, this is the first attempt to measure simultaneous changes in multiple phosphorylation sites of a newly characterized signaling protein. The method discerns differential phosphorylation to overall change in protein expression as reported previously for SILAC-based quantitation (43). Although phosphopeptide abundances are not reflective of the absolute levels of phosphorylation, most phosphorylation sites, including phosphopeptide consisting of Ser-202, show high levels of basal phosphorylation, suggesting that an increase in phosphorylation as a result of LPS stimulation becomes biologically significant and can regulate specific protein interactions. The SAS^{202}LASLYNGGLYNPYGR peptide shows a 2-fold increase in phosphorylation from both the label-free and AACT-based quantitation methods, suggesting that phosphorylation at Ser-202 is LPS-inducible. The mass spectrometry data were validated by both binding and NF-κB activity assays. In nonstimulated cells, LRRFIP2 is associated with the MyD88 complex that was found at a basal level in both the wild type and the S202A mutant. The LPS-induced, time course-dependent dynamics of the LRRFIP2-MyD88 interaction is closely correlated with that of site-specific phosphorylation(s) of LRRFIP2 determined by label-free quantitation. Correspondingly, the mutations of LRRFIP2 led to the loss of these LPS-induced dynamics, suggesting the unresponsive status of the macrophages to LPS. The phosphorylation of Ser-202 at LRRFIP2 apparently regulates the temporal interactions between LRRFIP2 and MyD88 that modulate the LPS-induced TLR4-mediated cellular response (12).

Strategically, we have demonstrated how a discovery-based mass spectrometry strategy with high precision can be utilized to characterize a novel role of site-specific phosphorylation and its dynamic interplay with specific protein-protein interactions for regulating signal transduction as well as for signal control. The accurate identification and quantification of site-specific phosphorylation, in this study, provided critical insights for guiding the concurrent biological characterization. These concerted discovery and biological characterization experiments implicate site-specific phosphorylation of LRRFIP2 as playing a pivotal role in modulating TLR4-mediated signaling.

REFERENCES

1. Liew, F. Y., Xu, D., Brint, E. K., and O'Neill, L. A. (2005) *Nat. Rev. Immunol.* **5,** 446–458
2. Dunne, A., and O'Neill, L. A. (2003) *Sci. STKE 2003,* re3
3. Janeway, C. A., Jr., and Medzhitov, R. (2002) *Annu. Rev. Immunol.* **20,** 197–216
4. Lee, M. S., and Kim, Y. J. (2007) *Annu. Rev. Biochem.* **76,** 447–480
5. O'Neill, L. A. (2003) *Biochem. Soc. Trans.* **31,** 643–647
6. Takeda, K., Kaisho, T., and Akira, S. (2003) *Annu. Rev. Immunol.* **21,** 335–376
7. Hatao, F., Yamamoto, M., Muroi, M., Kaminishi, M., and Tanamoto, K. (2008) *FEMS Immunol. Med. Microbiol.* **53,** 260–264
8. Verma, I. M., Stevenson, J. K., Schwarz, E. M., Van Antwerp, D., and Miyamoto, S. (1995) *Genes Dev.* **9,** 2723–2735
9. Wang, T., Gu, S., Ronni, T., Du, Y. C., and Chen, X. (2005) *J. Proteome Res.* **4,** 941–949
10. Du, Y. C., Gu, S., Zhou, J., Wang, T., Cai, H., Macinnes, M. A., Bradbury, E. M., and Chen, X. (2006) *Mol. Cell. Proteomics* **5,** 1033–1044
11. Povelones, M., Waterhouse, R. M., Kafatos, F. C., and Christophides, G. K. (2009) *Science* **324,** 258–261
12. Dai, P., Jeong, S. Y., Yu, Y., Leng, T., Wu, W., Xie, L., and Chen, X. (2009) *J. Immunol.* **182,** 3450–3460
13. Mann, M., Ong, S. E., Grønborg, M., Steen, H., Jensen, O. N., and Pandey, A. (2002) *Trends Biotechnol.* **20,** 261–268
14. Blume-Jensen, P., and Hunter, T. (2001) *Nature* **411,** 355–365
15. Faux, M. C., and Scott., J. D. (1996) *Trends Biol. Sci.* **21,** 312–315
16. Hunter, T. (1995) *Cell* **80,** 225–236
17. Krebs, E. G. (1994) *Trends Biochem. Sci.* **19,** 439–444
18. Olsen, J. V., Blagoev, B., Gnad, F., Macek, B., Kumar, C., Mortensen, P., and Mann, M. (2006) *Cell* **127,** 635–648
19. Chen, X., Smith, L. M., and Bradbury, E. M. (2000) *Anal. Chem.* **72,** 1134–1143
20. Zhu, H., Pan, S., Gu, S., Bradbury, E. M., and Chen, X. (2002) *Rapid Commun. Mass Spectrom.* **16,** 2115–2123
21. Ong, S. E., Blagoev, B., Kratchmarova, I., Kristensen, D. B., Steen, H., Pandey, A., and Mann, M. (2002) *Mol. Cell. Proteomics* **1,** 376–386
22. Zhu, H., Hunter, T. C., Pan, S., Yau, P. M., Bradbury, E. M., and Chen, X. (2002) *Anal. Chem.* **74,** 1687–1694
23. Gu, S., Wang, T., and Chen, X. (2008) *Proteomics* **8,** 3061–3070
24. Old, W. M., Meyer-Arendt, K., Aveline-Wolf, L., Pierce, K. G., Mendoza, A., Sevinsky, J. R., Resing, K. A., and Ahn, N. G. (2005) *Mol. Cell. Proteomics* **4,** 1487–1502
25. Resing, K. A., Johnson, R. S., and Walsh, K. A. (1995) *Biochemistry* **34,** 9477–9487
26. Ladner, R. D., Carr, S. A., Huddleston, M. J., McNulty, D. E., and Caradonna, S. J. (1996) *J. Biol. Chem.* **271,** 7752–7757
27. Wang, Y. K., Liao, P. C., Allison, J., Gage, D. A., Andrews, P. C., Lubman, D. M., Hanash, S. M., and Strahler, J. R. (1993) *J. Biol. Chem.* **268,** 14269–14277
28. Yip, T. T., and Hutchens, T. W. (1992) *FEBS Lett.* **308,** 149–153
29. Amankwa, L. N., Harder, K., Jirik, F., and Aebersold, R. (1995) *Protein Sci.* **4,** 113–125
30. Boersema, P. J., Mohammed, S., and Heck, A. J. (2009) *J. Mass Spectrom.* **44,** 861–878
31. Beausoleil, S. A., Jedrychowski, M., Schwartz, D., Elias, J. E., Villén, J., Li, J., Cohn, M. A., Cantley, L. C., and Gygi, S. P. (2004) *Proc. Natl. Acad. Sci. U.S.A.* **101,** 12130–12135
32. Schroeder, M. J., Shabanowitz, J., Schwartz, J. C., Hunt, D. F., and Coon, J. J. (2004) *Anal. Chem.* **76,** 3590–3598
33. Palumbo, A. M., and Reid, G. E. (2008) *Anal. Chem.* **80,** 9735–9747
34. Zubarev, R. A., Kruger, N. A., Fridriksson, E. K., Lewis, M. A., Horn, D. M., Carpenter, B. K., and McLafferty, F. W. (1999) *J. Am. Chem. Soc.* **121,** 2857–2862
35. Syka, J. E., Coon, J. J., Schroeder, M. J., Shabanowitz, J., and Hunt, D. F. (2004) *Proc. Natl. Acad. Sci. U.S.A.* **101,** 9528–9533
36. Gunawardena, H. P., Emory, J. F., and McLuckey, S. A. (2006) *Anal. Chem.* **78,** 3788–3793
37. Gunawardena, H. P., He, M., Chrisman, P. A., Pitteri, S. J., Hogan, J. M., Hodges, B. D., and McLuckey, S. A. (2005) *J. Am. Chem. Soc.* **127,** 12627–12639
38. McAlister, G. C., Phanstiel, D., Good, D. M., Berggren, W. T., and Coon, J. J. (2007) *Anal. Chem.* **79,** 3525–3534
39. Molina, H., Matthiesen, R., Kandasamy, K., and Pandey, A. (2008) *Anal. Chem.* **80,** 4825–4835
40. Kandasamy, K., Pandey, A., and Molina, H. (2009) *Anal. Chem.* **81,** 7170–7180
41. Shevchenko, A., Tomas, H., Havlis, J., Olsen, J. V., and Mann, M. (2006) *Nat. Protoc.* **1,** 2856–2860
42. Wolf-Yadlin, A., Hautaniemi, S., Lauffenburger, D. A., and White, F. M. (2007) *Proc. Natl. Acad. Sci. U.S.A.* **104,** 4860–4865
43. Olsen, J. V., Vermeulen, M., Santamaria, A., Kumar, C., Miller, M. L., Jensen, L. J., Gnad, F., Cox, J., Jensen, T. S., Nigg, E. A., Brunak, S., and Mann, M. (2010) *Sci. Signal. 2010,* ra3